Bell Inequalities and Quantum Correlations in $H \to ZZ \to 2e\,2\mu$

Mira Varma and Oliver K. Baker

Department of Physics, Yale University, New Haven, CT 06520, USA

mira.varma@yale.edu

February 19, 2025

Abstract

We investigate quantum correlations in Higgs-boson decays $\left(H \to ZZ^* \to 2e\,2\mu\right)$ using CMS open data at $\sqrt{s} = 8$ TeV, incorporating realistic detector effects. By reconstructing the polarization density matrix of the two-boson system and evaluating the Collins-Gisin-Linden-Massar-Popescu (CGLMP) Bell operator I_3, we quantify entanglement in the ZZ state. Our analysis yields an I_3 value of 2.152 ± 0.003 for signal events $\left(H \to ZZ^*\right)$, indicating the presence of quantum entanglement. The non-resonant continuum background events $\left(pp \to ZZ\right)$ yield $I_3 = 1.158 \pm 0.012$, suggesting the absence of quantum correlations. These results demonstrate the feasibility of testing fundamental quantum mechanics at high energy colliders.

1 Introduction

Quantum entanglement, a phenomenon at the heart of quantum mechanics [1, 2], has been extensively explored at low energies in systems such as photons [3], trapped ions [4], and superconducting qubits [5]. Only recently has it emerged as a powerful tool for probing particle interactions at much higher energies. This paper investigates quantum entanglement at the Large Hadron Collider (LHC), pushing our understanding of this quintessential quantum effect to unprecedented energy scales[1].

As Schrödinger once noted, entanglement is "not one but rather the characteristic trait of quantum mechanics" [7]. By studying entanglement at the LHC, we hope to leverage this key phenomenon to gain new insights into high-energy particle physics. Recent results from ATLAS [8] and CMS [9] have provided the first evidence of entanglement in top-quark pair production at the LHC. This follows earlier observations of Bell inequality violations [10]—fundamental tests of quantum correlations rooted in the Einstein-Podolsky-Rosen completeness paradox [11]—in particle physics using B-meson decays at LHCb and Belle II [12, 13]. These results demonstrate that quantum correlations persist at energies over

[1]For a recent comprehensive review of entanglement and Bell tests in high-energy collisions, see [6].

12 orders of magnitude [3, 14, 15, 16] higher than those in typical laboratory entanglement experiments.

Building on this foundation, we extend the study of quantum entanglement to the Higgs sector, focusing on the decay channel $H \to ZZ^* \to 2e\,2\mu$, with the $pp \to ZZ$ process serving as the primary background. Recent theoretical work suggests this channel is particularly promising for observing Bell inequality violations [17, 18], with predictions pointing toward potential observations at the HL-LHC. The four-lepton final state offers a clean experimental signature [19] where the complete kinematics can be reconstructed, making it ideal for quantum state analysis [20, 21].

It is important to note that a comprehensive study of Bell's inequality in the $H \to ZZ \to 4\ell$ channel ultimately requires the inclusion of higher-order QCD and electroweak corrections, off-shell modeling, and well-defined fiducial selections, as discussed in Ref. [22]. In this work, however, our focus is on demonstrating feasibility at the detector level, so we do not incorporate these additional effects.

The theoretical framework for analyzing entanglement in $H \to ZZ^*$ has been developed in several recent papers. The construction of the appropriate Bell operators was outlined in [17], while comprehensive analytical predictions for the polarization density matrix were provided in [23]. The quantum tomography techniques required for reconstructing density matrices from experimental data were detailed in [18]. For related proposals to perform quantum tomography in collider physics, see Refs. [24, 25, 26], which focus on top-quark pair production and spin-state reconstruction using quantum-information methods.

In our approach, we employ the polarization density matrix reconstruction technique developed by [23] using CMS open data. This marks the first attempt to apply these theoretical methods to $H \to ZZ \to 4\ell$ collider data that includes detector effects. By computing the Bell operator expectation value I_3, we aim to quantify the quantum correlations and test the completeness of quantum mechanics at these high energies.

This work has the potential to:

1. Extend our understanding of quantum entanglement to unprecedented energies,
2. Provide new tests of quantum mechanics in extreme environments,
3. Offer novel probes of the Higgs boson's properties and interactions, and
4. Bridge the gap between quantum information theory and high-energy particle physics.

While previous studies have been either purely theoretical or based on truth-level Monte Carlo simulations, this work demonstrates the feasibility of reconstructing the polarization density matrix using simulated data that includes detector effects. Although using an outreach dataset limits the statistical precision possible, successfully implementing these techniques with detector-level events represents an important step toward future measurements of quantum correlations in the Higgs sector using actual collision data.

2 Background

Our work leverages the fact that massive spin-1 bosons, like the Z-bosons produced in Higgs decays or non-resonant di-boson processes, can exhibit quantum correlations beyond any clas-

sical description. We adopt the density matrix formalism, using simulation-level data that include realistic detector effects—making our analysis especially relevant for experimental high-energy physics. While some earlier studies rely on truth-level data alone [17, 18, 23, 27, 28], we account for the complexities introduced by the detector.

2.1 Quantum State of the Di-boson System

In quantum mechanics, the state of a system is fully described by its density matrix, ρ. A state is said to be pure if it can be represented by a single state vector:

$$\rho = |\psi\rangle\langle\psi|, \tag{1}$$

which satisfies $\rho^2 = \rho$ and $\mathrm{Tr}(\rho^2) = 1$. In contrast, a mixed state is a statistical ensemble of pure states, weighted by probabilities p_i:

$$\rho = \sum_i p_i \, |\psi_i\rangle\langle\psi_i|, \tag{2}$$

where $\mathrm{Tr}(\rho^2) < 1$.

When a Higgs boson decays into a Z and a Z^*-boson, the spin state of the two-boson system in the helicity basis is [23, 27]:

$$|\Psi\rangle = \frac{1}{\sqrt{2+\varkappa^2}}\Big[|+,-\rangle - \varkappa\,|0,0\rangle + |-,+\rangle\Big], \tag{3}$$

where $|+,-\rangle$, $|0,0\rangle$, and $|-,+\rangle$ denote helicity configurations $(+1,-1)$, $(0,0)$, and $(-1,+1)$ for the two Z-bosons. The parameter $\varkappa$ depends on the kinematics:

$$\varkappa = 1 + \frac{m_H^2 - (1+(M_V^*/M_V))^2 M_V^2}{2(M_V^*/M_V)M_V^2}, \tag{4}$$

where m_H is the Higgs mass, M_V is the on-shell Z-mass, and M_V^* is the Z^*-mass. When $\varkappa = 1$, Eq. (3) reduces to a maximally entangled spin singlet:

$$|\Psi\rangle = \frac{1}{\sqrt{3}}\left(|1,-1\rangle - |0,0\rangle + |-1,1\rangle\right). \tag{5}$$

An important point is that while individual events correspond to pure states, our measurement involves an ensemble of events with different $\varkappa$ values, determined by the kinematics of each decay. This means we are effectively measuring a mixture of states with different Z^*-masses, rather than the idealized case, where $\varkappa = 1$. To minimize ambiguities in reconstructing these states, we focus on the $2e2\mu$ channel, where the lepton pairing clearly identifies each parent Z-boson.

2.2 The Density Matrix Formalism

2.2.1 Single-Boson Polarization Density Matrix

A single massive spin-1 boson, such as the Z, can be described by a 3×3 polarization density matrix, $\rho_{\lambda\lambda'}$, with elements:

$$\rho_{\lambda\lambda'} = \frac{\mathcal{M}(\lambda)\mathcal{M}^*(\lambda')}{\sum_\lambda |\mathcal{M}(\lambda)|^2}, \tag{6}$$

where $\mathcal{M}(\lambda)$ is the helicity amplitude for state λ, with $\lambda, \lambda' \in \{-1, 0, +1\}$. The diagonal entries $\rho_{\lambda\lambda}$ represent the probabilities of the boson being in a given helicity state, while off-diagonal elements ($\lambda \neq \lambda'$) reveal quantum correlations within the system.

2.2.2 Two-Boson Density Matrix

When two spin-1 bosons (e.g., Z-bosons) appear simultaneously, such as in $H \to ZZ^*$ or non-resonant ZZ production, their joint quantum state resides in a $3 \otimes 3$ Hilbert space, described by a 9×9 density matrix $\rho_{(2)}$[2]. One can expand in terms of the Gell-Mann basis $(T^a, a = 1, \ldots, 8)$ and the identity matrix $\mathbb{I}$:

$$\rho_{(2)} = \left(\frac{1}{9}\left[\mathbb{I} \otimes \mathbb{I}\right] + \sum_{a=1}^{8} f_a \left[T^a \otimes \mathbb{I}\right] + \sum_{b=1}^{8} g_b \left[\mathbb{I} \otimes T^b\right] + \sum_{a,b=1}^{8} h_{ab} \left[T^a \otimes T^b\right] \right)_{\lambda_1, \lambda_1', \lambda_2, \lambda_2'} . \quad (7)$$

Here, f_a represents the polarization of the first Z-boson, g_b represents the polarization of the second Z-boson, and h_{ab} describes the joint correlation between the two bosons. Note that f_a, g_b, and h_{ab} are all real numbers. The off-diagonal elements in $\rho_{(2)}$ encode quantum correlations, including entanglement. In matrix form, $\rho_{(2)}$ can be written as [23]:

$$\rho_H = 2 \begin{pmatrix} 0 & 0 & 0 & 0 & 0 & 0 & 0 & 0 & 0 \\ 0 & 0 & 0 & 0 & 0 & 0 & 0 & 0 & 0 \\ 0 & 0 & h_{44} & 0 & h_{16} & 0 & h_{44} & 0 & 0 \\ 0 & 0 & 0 & 0 & 0 & 0 & h_{44} & 0 & 0 \\ 0 & 0 & h_{16} & 0 & 2h_{33} & 0 & h_{16} & 0 & 0 \\ 0 & 0 & 0 & 0 & 0 & 0 & 0 & 0 & 0 \\ 0 & 0 & h_{44} & 0 & h_{16} & 0 & h_{44} & 0 & 0 \\ 0 & 0 & 0 & 0 & 0 & 0 & 0 & 0 & 0 \\ 0 & 0 & 0 & 0 & 0 & 0 & 0 & 0 & 0 \end{pmatrix} \quad (8)$$

.

For $H \to ZZ^*$, the key non-zero elements are:

$$\begin{aligned} h_{16} = h_{61} = h_{27} = h_{72} &= \frac{f M_V^2 \left[-m_H^2 + (1 + f^2) M_V^2\right]}{D}, \\ h_{33} &= \frac{1}{4} \frac{\left[m_H^2 - (1 + f^2) M_V^2\right]^2}{D}, \\ h_{44} &= \frac{2 f^2 M_V^4}{D}, \end{aligned} \quad (9)$$

where,

- $f = M_Z^*/M_Z$ is the mass ratio of the off-shell to on-shell Z-boson
- $D = m_H^4 - 2\,(1 + f^2)\, m_H^2 M_V^2 + (1 + 10 f^2 + f^4)\, M_V^4$ is the denominator
- M_V^2 represents the vector (in this case Z-boson) mass

[2]See Refs. [17, 29, 30] for related discussions of spin-1 entangled states in collider processes.

2.3 Bell Inequalities for Spin-1 Particles

In the case of two spin-1 particles, we can employ the Collins–Gisin–Linden–Massar–Popescu inequality [31, 32], which extends Bell tests to three-level (qutrit) systems. Its associated Bell observable, I_3, is computed via polarization density matrix coefficients.

1. If $I_3 \leq 2$, the correlations in can be explained by local hidden-variable models, suggesting quantum mechanics may be incomplete.

2. If $I_3 > 2$, the Bell inequality is violated, indicating quantum entanglement.

Our study finds $I_3 > 2$ predominantly in Higgs-mediated ($H \to ZZ^*$) processes, while the continuum ZZ^* fails to reach this threshold. Since we work at detector level, these results are particularly relevant to potential future experimental measurements.

2.3.1 Bell's Inequality from Density Matrix Coefficients

In our formalism, the CGLMP operator I_3 is defined in terms of the density matrix coefficients [23]:

$$I_3 = 4\,(h_{44} + h_{55}) - \frac{4\sqrt{3}}{3}\,[h_{61} + h_{66} + h_{72} + h_{77} + h_{11} + h_{16} + h_{22} + h_{27}] \tag{10}$$

The general form of the Bell operator I_3 can be simplified using symmetries of the $H \to ZZ^*$ system. From the symmetries of the decay, we have $h_{16} = h_{61} = h_{27} = h_{72}$, $h_{38} = h_{83}$, and $h_{44} = h_{55}$. Substituting these relations into the above equation gives us the simplified expression for I_3 [23]:

$$I_3 = 8h_{44} - \frac{16}{\sqrt{3}}h_{16} \tag{11}$$

2.4 Reconstruction from Lepton Decay Angles

When each Z-boson decays to a lepton pair, the resulting daughter particles ($\ell^+\ell^-$) encode spin information about the original boson. We reconstruct their four-momenta in the lab frame using standard formulas[3]:

$$\begin{aligned} p_x &= p_T \cos(\phi), \\ p_y &= p_T \sin(\phi), \\ p_z &= p_T \sinh(\eta), \\ E &= \sqrt{p_x^2 + p_y^2 + p_z^2 + m^2}. \end{aligned} \tag{12}$$

We then boost into the Higgs rest frame to identify Z-boson momenta:

$$p_{Z1} = p_{\ell 1} + p_{\ell 2}, \quad p_{Z2} = p_{\ell 3} + p_{\ell 4}.$$

[3] If one is unfamiliar with these relations, Ref. [33] is an excellent resource.

From these momenta, we compute the invariant masses m_{Z1} and m_{Z2}. To reconstruct the polarization density matrix, the only experimental input we need is the ratio f:

$$f = \frac{m_{Z2}}{m_{Z1}}. \tag{13}$$

Boosting further into each Z-rest frame, we obtain the polar (θ) and azimuthal (ϕ) angles of the negatively charged lepton:

$$\theta_{Z_{1,2}} = \arccos\left(\frac{p_{z_{Z_{1,2}}}}{\sqrt{p^2_{x_{Z_{1,2}}} + p^2_{y_{Z_{1,2}}} + p^2_{z_{Z_{1,2}}}}}\right), \quad \phi_{Z_{1,2}} = \arctan\left(\frac{p_{y_{Z_{1,2}}}}{p_{x_{Z_{1,2}}}}\right),$$

where the momenta components are those of the negatively charged leptons in their respective parent Z-boson rest frames.

3 Data and Methodology

We analyze publicly available CMS Open Data [34, 35] at $\sqrt{s} = 8$ TeV, containing both Higgs boson decays and non-resonant ZZ^* production under realistic detector conditions[4].

For the signal, we analyzed $H \to ZZ^* \to 4\ell$ events, where the final-state leptons consisted of two electrons and two muons ($2e2\mu$). This final state was chosen to avoid ambiguities in identifying which leptons originated from which Z-boson, an issue that arises in events with four same-flavor leptons. Events were generated using the POWHEG event generator, with PYTHIA6 applied for parton showering. The full dataset contained 299,973 events, of which 27,945 were analyzed to ensure a balanced comparison with the filtered background dataset, described below.

For the background, we considered non-resonant $ZZ^* \to 4\ell$ production ($pp \to ZZ^* \to 4\ell$) under identical simulation conditions. This process constitutes the primary background for $H \to ZZ^* \to 4\ell$, as it produces the same final state without involving an intermediate Higgs boson. The dataset included 1,497,445 events, focusing on the same $2e2\mu$ final state as the signal.

To isolate events consistent with the $H \to ZZ^* \to 4\ell$ process and the ZZ^* background, we applied a filtering criterion based on the sum of the invariant masses of the two Z-bosons:

$$120\,\text{GeV} \leq M_{Z1} + M_{Z2} \leq 130\,\text{GeV}.$$

This filter was chosen to isolate events consistent with the kinematics of $H \to ZZ^* \to 4\ell$ decays, as the Higgs boson mass is approximately 125 GeV. Since the background dataset represents non-resonant ZZ^* production, it contains events across a wide range of kinematics. The filter suppresses contributions from events outside the Higgs mass range, ensuring that the remaining background events closely resemble those expected in Higgs decays. The filtering criterion was applied uniformly to both the signal and background datasets to isolate events consistent with the expected kinematics of $H \to ZZ^* \to 4\ell$ decays. All results presented in this paper use this Z-boson sum mass selection criterion.

[4]These datasets were derived from primary CMS datasets in AOD format, which were validated by the CMS collaboration. The reduced NanoAOD format retains key kinematic and detector-level information and has been optimized for education and outreach purposes.

4 Results

4.1 Bell Operator I_3

Figure 1 shows the measured Bell operator I_3 for signal (orange) and background (blue) events. For the signal dataset, we measure $I_3 = 2.152 \pm 0.003$, exceeding the classical limit of $I_3 = 2$ and demonstrating Bell's inequality violation. For background events, we obtain $I_3 = 1.158 \pm 0.012$, well below the classical threshold. The stark difference between these two values reinforces the presence of entanglement in the Higgs-mediated channel. The quantum mechanical upper limit of $I_3 = 2\sqrt{2} \approx 2.83$ is shown for reference. It is important to note that since I_3 is an ensemble averaged quantity, only the averaged I_3 holds physical significance. In the following sections, we plot I_3 vs angular and kinematic variables, respectively, to highlight trends and correlations.

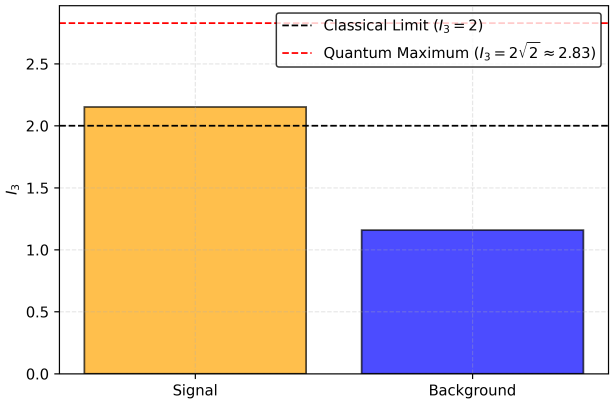

Figure 1: Measured Bell operator I_3 values for signal (orange) and background (blue) events in the 120–130 GeV mass window. The signal events yield $I_3 = 2.152 \pm 0.003$, showing clear Bell inequality violation ($I_3 > 2$), while background events give $I_3 = 1.158 \pm 0.012$. The classical limit ($I_3 = 2$) and quantum mechanical maximum ($I_3 = 2\sqrt{2} \approx 2.83$) are shown as dashed lines.

4.2 Angular Distributions and Correlations

Figure 2 presents the polar (θ_{Z1}, θ_{Z2}) and azimuthal (ϕ_{Z1}, ϕ_{Z2}) distributions for both signal and background. The polar angles exhibit broad peaks between 75° and 100°, diminishing near 0° or 180°. The azimuthal angles appear nearly uniform. The azimuthal angle distributions remain approximately uniform over the range −180° to 180° for both samples.

The dependence of the Bell operator I_3 on these angular variables was also examined (Fig. 3) to identify possible angular effects on Bell inequality violation. For the signal dataset, strong violations of the Bell inequality ($I_3 > 2$) are observed across all angular ranges. However, slight reductions in I_3 values are present near the polar angle extremes. No such reduction is observed for the azimuthal angles, where I_3 values remain uniform across the range.

The background events, however, display I_3 values ranging from 0 to approximately 2.2, showing no significant correlation with any angular variables.

4.3 Mass Distributions and Bell Operator Correlations

Figure 5 illustrates the dependence of the Bell operator I_3 on kinematic variables (m_{Z2}, m_{ZZ}, and p_T^{miss}). Signal events consistently exhibit $I_3 > 2$, with a higher density observed at m_{Z2} between 20 GeV and 40 GeV, and clustering at m_{ZZ} in the range 87 GeV to 95 GeV. Background events remain below the threshold, showing no significant correlation with these variables.

The variation of I_3 with missing transverse momentum (p_T^{miss}) is also shown in Figure 5. Signal events show $I_3 > 2$ across the entire p_T^{miss} range, with a higher density of violations for $p_T^{miss} \leq 30$ GeV. Background events maintain consistently low I_3 values regardless of p_T^{miss}, further highlighting the absence of quantum correlations in non-signal processes.

4.4 Density Matrices for Signal and Background Samples

After aggregating events in the 120 GeV $\leq m_{ZZ} \leq$ 130 GeV window, we average over all reconstructed events to obtain the final density matrices. Below are the numerical results for the signal channel ($H \to ZZ^*$) and the continuum background ($pp \to ZZ^*$). These matrices are written in the helicity basis $\{|+1,+1\rangle, |+1,0\rangle, \ldots, |-1,-1\rangle\}$ with indices running from 1 to 9. The magnitude of off-diagonal elements indicates the strength of quantum correlations between the Z-bosons, with larger values in the signal suggesting stronger entanglement.

Signal Matrix (ρ_{signal}):

$$\rho_{\text{signal}} = 2 \begin{pmatrix} 0 & 0 & 0 & 0 & 0 & 0 & 0 & 0 & 0 \\ 0 & 0 & 0 & 0 & 0 & 0 & 0 & 0 & 0 \\ 0 & 0 & 0.1058 & 0 & -0.2448 & 0 & 0.1058 & 0 & 0 \\ 0 & 0 & 0 & 0 & 0 & 0 & 0 & 0 & 0 \\ 0 & 0 & -0.2448 & 0 & 0.2884 & 0 & -0.2448 & 0 & 0 \\ 0 & 0 & 0 & 0 & 0 & 0 & 0 & 0 & 0 \\ 0 & 0 & 0.1058 & 0 & -0.2448 & 0 & 0.1058 & 0 & 0 \\ 0 & 0 & 0 & 0 & 0 & 0 & 0 & 0 & 0 \\ 0 & 0 & 0 & 0 & 0 & 0 & 0 & 0 & 0 \end{pmatrix}. \tag{14}$$

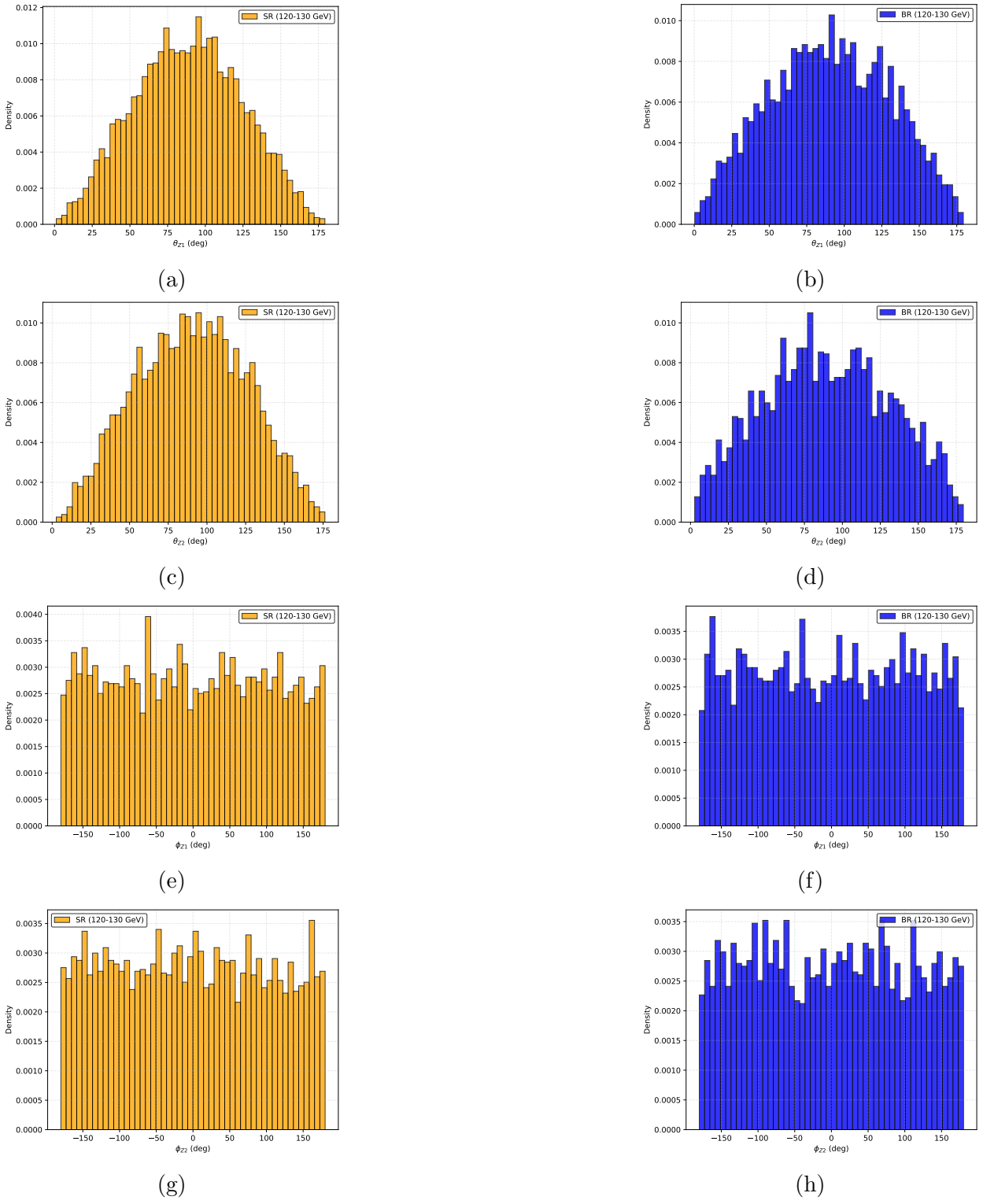

Figure 2: Angular distributions for signal (orange) and background (blue) events in the mass window 120 GeV $\leq m_{ZZ} \leq$ 130 GeV. Top row: polar angle distributions for (a) θ_{Z1} signal, (b) θ_{Z1} background, (c) θ_{Z2} signal, and (d) θ_{Z2} background. Bottom row: azimuthal angle distributions for (e) ϕ_{Z1} signal, (f) ϕ_{Z1} background, (g) ϕ_{Z2} signal, and (h) ϕ_{Z2} background.

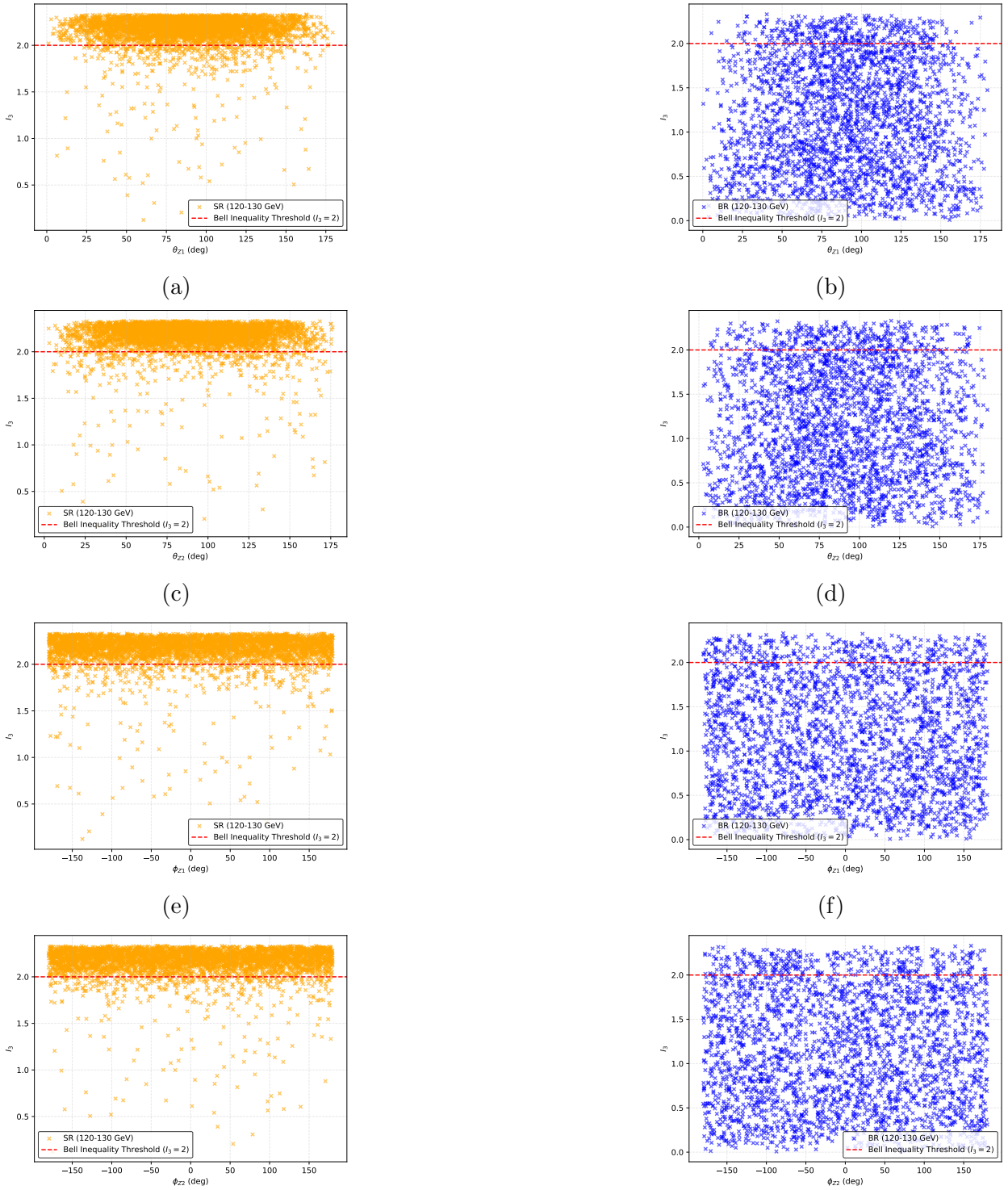

Figure 3: Bell operator I_3 correlations with angular variables for signal (orange) and background (blue) events. The red dashed line indicates the Bell inequality threshold ($I_3 = 2$). Correlation with polar angles: (a) θ_{Z1} signal, (b) θ_{Z1} background, (c) θ_{Z2} signal, (d) θ_{Z2} background. Correlation with azimuthal angles: (e) ϕ_{Z1} signal, (f) ϕ_{Z1} background, (g) ϕ_{Z2} signal, (h) ϕ_{Z2} background.

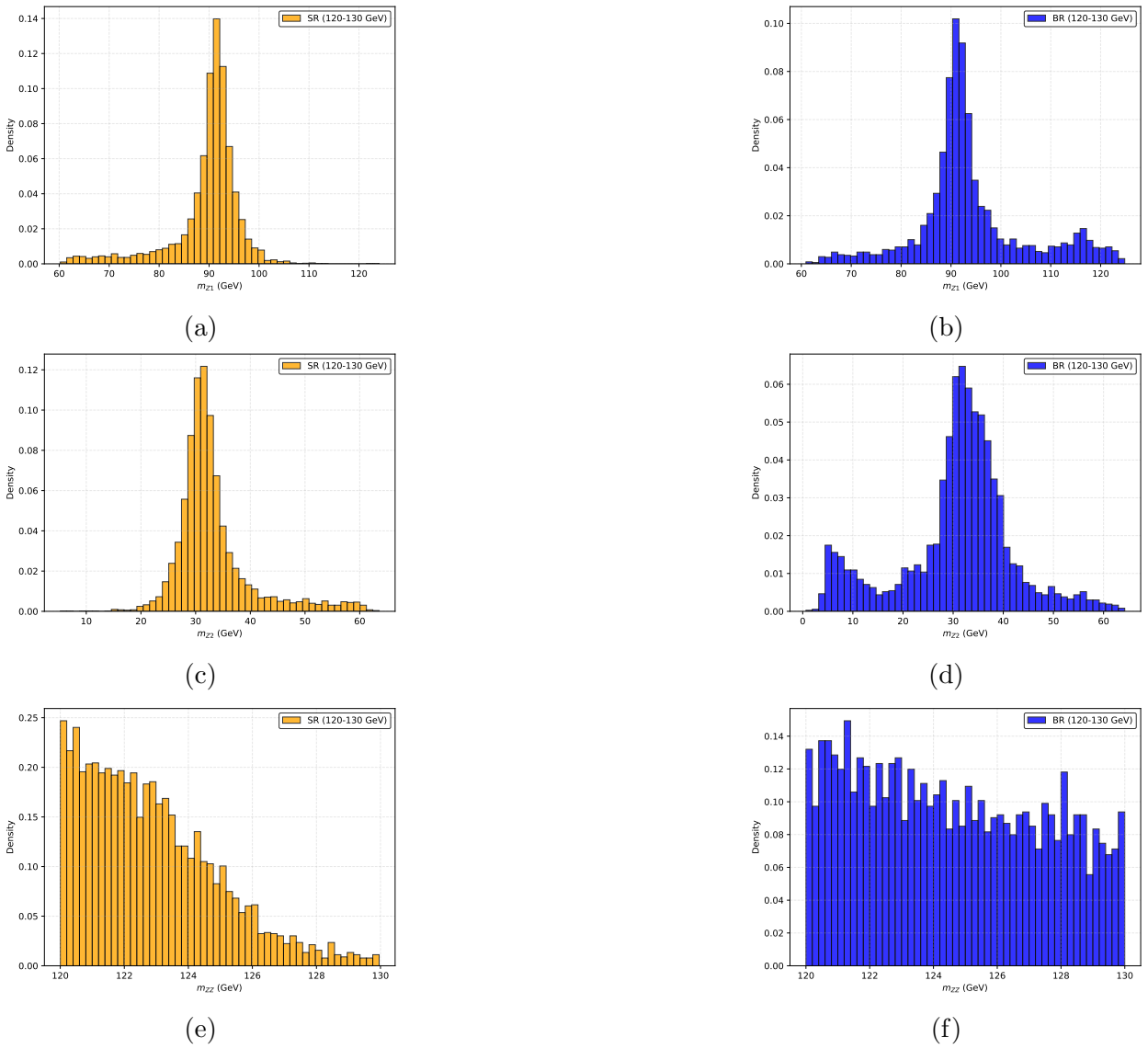

Figure 4: Mass distributions in the 120 GeV $\leq m_{ZZ} \leq$ 130 GeV window. On-shell Z-boson mass (m_{Z1}) for (a) signal ($\langle m_{Z1} \rangle = 89.67 \pm 0.10$ GeV) and (b) background ($\langle m_{Z1} \rangle = 93.72 \pm 0.21$ GeV). Off-shell Z-boson mass (m_{Z2}) for (c) signal ($\langle m_{Z2} \rangle = 33.14 \pm 0.10$ GeV) and (d) background ($\langle m_{Z2} \rangle = 30.83 \pm 0.21$ GeV). Four-lepton invariant mass (m_{ZZ}) for (e) signal ($\langle m_{ZZ} \rangle = 122.81 \pm 0.14$ GeV) and (f) background ($\langle m_{ZZ} \rangle = 124.54 \pm 0.30$ GeV).

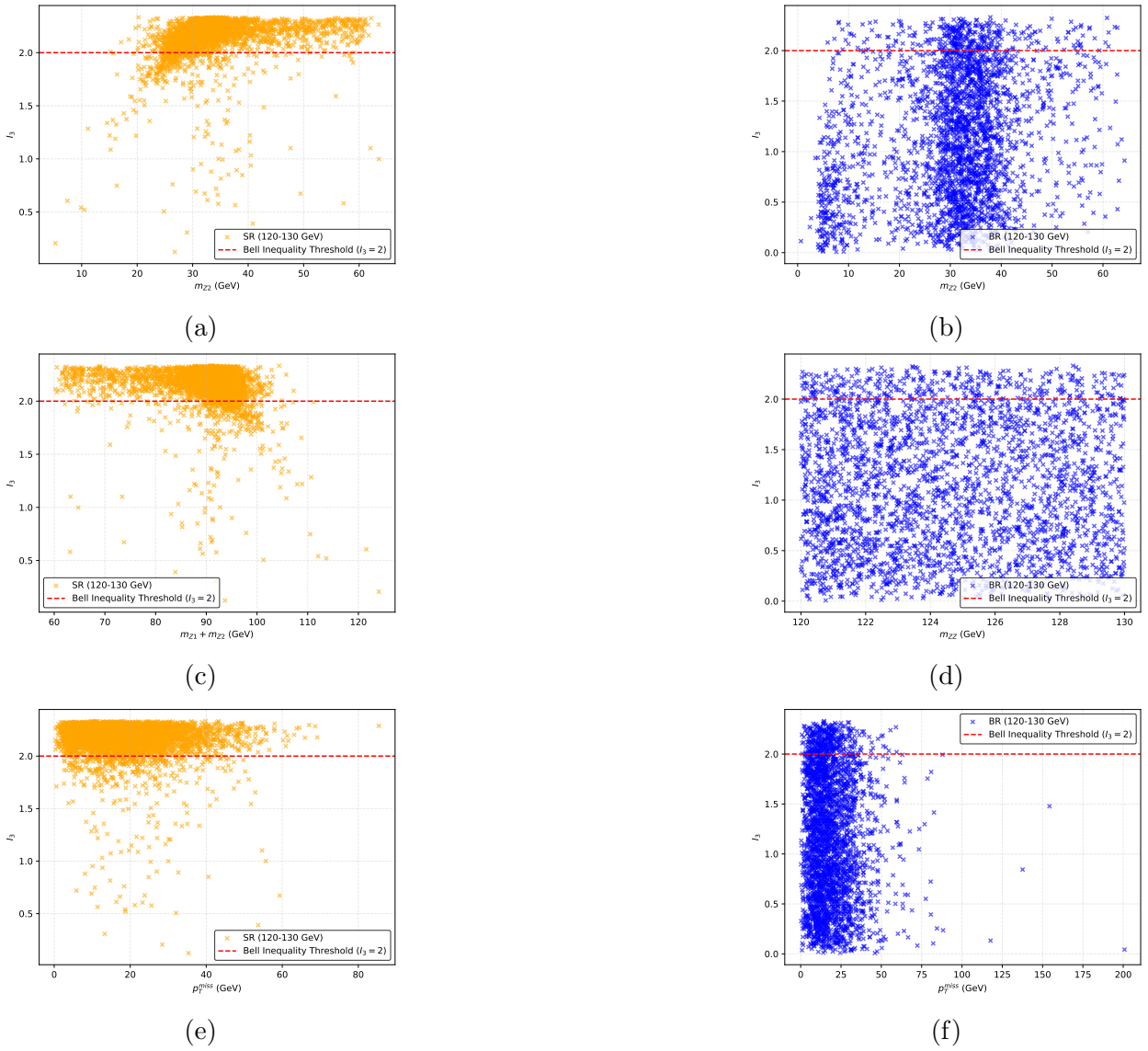

Figure 5: Bell operator I_3 dependence on kinematic variables for signal (orange) and background (blue) events. The red dashed line indicates $I_3 = 2$. (a,b) I_3 versus m_{Z2}, showing signal clustering at 20–40 GeV. (c,d) I_3 versus m_{ZZ}, with strong violations at 87–95 GeV. (e,f) I_3 versus p_T^{miss}, with signal events maintaining $I_3 > 2$ and clustering below 30 GeV.

Background Matrix (ρ_{bkg}):

$$\rho_{\text{bkg}} = 2 \begin{pmatrix} 0 & 0 & 0 & 0 & 0 & 0 & 0 & 0 & 0 \\ 0 & 0 & 0 & 0 & 0 & 0 & 0 & 0 & 0 \\ 0 & 0 & 0.0405 & 0 & -0.1563 & 0 & 0.0405 & 0 & 0 \\ 0 & 0 & 0 & 0 & 0 & 0 & 0 & 0 & 0 \\ 0 & 0 & -0.1563 & 0 & 0.4189 & 0 & -0.1563 & 0 & 0 \\ 0 & 0 & 0 & 0 & 0 & 0 & 0 & 0 & 0 \\ 0 & 0 & 0.0405 & 0 & -0.1563 & 0 & 0.0405 & 0 & 0 \\ 0 & 0 & 0 & 0 & 0 & 0 & 0 & 0 & 0 \\ 0 & 0 & 0 & 0 & 0 & 0 & 0 & 0 & 0 \end{pmatrix}. \tag{15}$$

Following the standard convention for spin-1 entangled systems [23], we multiply the reconstructed density matrices by a factor of 2 to ensure this normalization in the helicity basis. For the $Z_1 + Z_2$ mass filtering, the averaged density matrix was found to satisfy $\text{Tr}(\rho) = 1$, indicating proper normalization and a consistent quantum state representation.

In contrast, alternative filtering methods, such as Higgs mass filtering, produced $\text{Tr}(\rho) \neq 1$, highlighting the reliability of the $Z_1 + Z_2$ mass filtering. The off-diagonal elements, representing quantum coherence, are significantly larger for the signal sample, reflecting the presence of strong quantum entanglement in $H \to ZZ^* \to 4\ell$ decays. This quantum coherence is absent in the background, highlighting the fundamental differences between resonant Higgs production and non-resonant di-boson processes.

4.5 Interpretation of Off-Diagonal Elements

The non-zero off-diagonal elements in the density matrices quantify quantum correlations between different helicity states of the Z-bosons. In the signal sample, these elements are larger because the spin-0 Higgs boson must decay to a specific quantum superposition of ZZ^* helicity states to conserve angular momentum. Comparing the matrices, we observe that the off-diagonal elements in the signal are approximately twice the magnitude of those in the background, indicating stronger entanglement between the Z-bosons in Higgs decays. The smaller off-diagonal elements in the background process occur since the Z-bosons are produced directly in pp collisions without constraints from an intermediate resonance, resulting in weaker quantum correlations.

4.6 Statistical Uncertainties

The statistical uncertainties on the non-zero elements of ρ_{signal} are:

- $\rho_{3,3} = \rho_{3,7} = \rho_{7,3} = \rho_{7,7} = 0.105805 \pm 0.000225$
- $\rho_{3,5} = \rho_{5,3} = \rho_{5,7} = \rho_{7,5} = -0.244798 \pm 0.000208$
- $\rho_{5,5} = 0.28839 \pm 0.000225$

Similarly, for ρ_{bkg}:

- $\rho_{3,3} = \rho_{3,7} = \rho_{7,3} = \rho_{7,7} = 0.040539 \pm 0.000635$
- $\rho_{3,5} = \rho_{5,3} = \rho_{5,7} = \rho_{7,5} = -0.156318 \pm 0.001303$
- $\rho_{5,5} = 0.418922 \pm 0.000635$

5 Discussion

This study demonstrates significant violations of the Bell inequality in $H \to ZZ^* \to 4\ell$ decays, as evidenced by the distribution of the Bell operator I_3. The finding that $I_3 = 2.152 \pm 0.003$ for signal events, which exceeds the classical threshold of $I_3 = 2$, provides strong evidence for the presence of quantum entanglement in this process, even in the presence of detector effects. One may notice that although we do see entanglement, the measured I_3 value still falls short of the quantum mechanical maximum ($I_3 = 2\sqrt{2} \approx 2.83$). his is expected, as introducing detector effects can weaken the quantum correlations needed for maximal Bell inequality violation.

We explored an alternative selection based directly on the Higgs mass (120 GeV $\leq m_H \leq$ 130 GeV). This method, however, produced an unphysical signal density matrix with $\mathrm{Tr}(\rho) \neq 1$, indicating an improper quantum state. We instead selected events based on the sum of Z-boson masses, which better isolated signal events from background processes, as evidenced by the proper normalization $\mathrm{Tr}(\rho) = 1$ and the clear separation between signal and background quantum correlations. This is particularly apparent in the density matrix off-diagonal elements, which are significantly larger for the signal sample, reflecting the strong quantum entanglement expected in Higgs-mediated decays.

The angular dependence of I_3 reveals notable differences. Polar angles (θ_{Z1}, θ_{Z2}) show a slight reduction in I_3 near the extremes, possibly reflecting spin correlations in the Higgs rest frame. Azimuthal angles (ϕ_{Z1}, ϕ_{Z2}) show no such dependence, suggesting that these angles are less sensitive to spin effects.

The clustering of $I_3 > 2$ events in specific mass ranges (e.g., 20–40 GeV for m_{Z2} and 87–95 GeV for m_{ZZ}) underscores regions of heightened quantum correlations. These patterns are absent in the background, emphasizing sensitivity to entanglement in the signal process. While this analysis focuses on statistical uncertainties, several systematic effects could influence these measurements, including detector resolution and acceptance effects in lepton reconstruction, and uncertainties in background modeling. A detailed study of these systematic uncertainties and their impact on density matrix reconstruction is beyond the scope of this paper but will be important for future measurements with collision data [22].

6 Conclusion

In this work, we have reconstructed the polarization density matrix for both the signal channel $\left(H \to ZZ^* \to 4\ell\right)$ and the non-resonant continuum background $\left(pp \to ZZ^* \to 4\ell\right)$ using CMS open source data that incorporates realistic detector effects. Focusing on the mass window 120 GeV $\leq m_{ZZ} \leq$ 130 GeV, our results indicate that $I_3 = 2.152 \pm 0.003$ for signal events, above the Bell-inequality threshold $I_3 = 2$. Under the same analysis procedure,

background events yield $I_3 = 1.158 \pm 0.012$. This difference underscores the presence of quantum correlations, namely quantum entanglement, in Higgs-mediated di-boson decays.

Despite these encouraging observations, one must recall that Bell's inequality tests are subject to several well-known loopholes. First, the detection loophole arises because only a fraction of events are recorded [36], although the high efficiency of modern detectors partially mitigates this concern. Second, the locality loophole questions whether particles are sufficiently isolated from classical interactions that could mimic entanglement; robust event selection and particle identification can partially alleviate this concern [10]. Third, the coincidence loophole—the possibility of incorrectly pairing final-state particles—can be addressed by careful momentum reconstruction and by using a large ensemble of events, diluting any mislabeling biases [37]. Finally, the freedom-of-choice loophole questions whether measurement choices are truly independent. At a collider, detector configurations are largely fixed, making this the hardest loophole to avoid [38].

Our findings indicate that realistic detector conditions do not appear to significantly obstruct the detection of quantum correlations in Higgs-mediated ZZ^* decays. We observe robust Bell inequality violations in the signal region, suggesting that such studies are indeed feasible at LHC energies. Future work will aim to improve background modeling, extend the analysis to additional invariant mass or angular regions where entanglement could be better highlighted, and explore strategies to address the remaining loopholes more definitively (particularly the freedom-of-choice loophole). Although substantial work remains, this study represent a significant step toward demonstrating the viability of probing quantum correlations in high-energy colliders.

Acknowledgments

The authors thank the ATLAS HZZ Working Group for valuable discussions that helped shape this analysis, as well as J. A. Aguilar-Saavedra for his helpful feedback on our draft. We also acknowledge the CMS Collaboration for their commitment to open science and for making their data publicly available, which enabled this independent investigation of quantum entanglement. The authors gratefully acknowledge funding support from the U.S. Department of Energy, Office of Science, under Award DE-FG02-92ER40704.

References

[1] Ryszard Horodecki, Pawel Horodecki, Michal Horodecki, and Karol Horodecki. Quantum entanglement. *Rev. Mod. Phys.*, 81:865–942, 2009. DOI: 10.1103/RevModPhys.81.865.

[2] Nicolas Brunner, Daniel Cavalcanti, Stefano Pironio, Valerio Scarani, and Stephanie Wehner. Bell nonlocality. *Rev. Mod. Phys.*, 86:419, 2014. DOI: 10.1103/RevModPhys.86.419.

[3] Alain Aspect, Jean Dalibard, and Gerard Roger. Experimental test of Bell's inequalities

using time varying analyzers. *Phys. Rev. Lett.*, 49:1804–1807, 1982. DOI: 10.1103/PhysRevLett.49.1804.

[4] J. I. Cirac and P. Zoller. Quantum Computations with Cold Trapped Ions. *Phys. Rev. Lett.*, 74:4091–4094, 1995. DOI: 10.1103/PhysRevLett.74.4091.

[5] Alexandre Blais, Ren-Shou Huang, Andreas Wallraff, S. M. Girvin, and R. J. Schoelkopf. Cavity quantum electrodynamics for superconducting electrical circuits: An architecture for quantum computation. *Phys. Rev. A*, 69(6):062320, 2004. DOI: 10.1103/PhysRevA.69.062320.

[6] Alan J. Barr, Marco Fabbrichesi, Roberto Floreanini, Emidio Gabrielli, and Luca Marzola. Quantum entanglement and Bell inequality violation at colliders. *Prog. Part. Nucl. Phys.*, 139:104134, 2024. DOI: 10.1016/j.ppnp.2024.104134.

[7] E. Schrodinger. Die gegenwartige Situation in der Quantenmechanik. *Naturwiss.*, 23: 807–812, 1935. DOI: 10.1007/BF01491891.

[8] Georges Aad et al. Observation of quantum entanglement in top-quark pairs using the ATLAS detector. 11 2023.

[9] Aram Hayrapetyan et al. Observation of quantum entanglement in top quark pair production in proton–proton collisions at $\sqrt{s} = 13$ TeV. *Rept. Prog. Phys.*, 87(11): 117801, 2024. DOI: 10.1088/1361-6633/ad7e4d.

[10] J. S. Bell. On the Einstein-Podolsky-Rosen paradox. *Physics Physique Fizika*, 1:195–200, 1964. DOI: 10.1103/PhysicsPhysiqueFizika.1.195.

[11] Albert Einstein, Boris Podolsky, and Nathan Rosen. Can quantum mechanical description of physical reality be considered complete? *Phys. Rev.*, 47:777–780, 1935. DOI: 10.1103/PhysRev.47.777.

[12] M. Fabbrichesi, R. Floreanini, E. Gabrielli, and L. Marzola. Bell inequality is violated in B0→J/ψK*(892)0 decays. *Phys. Rev. D*, 109(3):L031104, 2024. DOI: 10.1103/PhysRevD.109.L031104.

[13] Emidio Gabrielli and Luca Marzola. Entanglement and Bell Inequality Violation in B $\to \phi\phi$ Decays. *Symmetry*, 16(8):1036, 2024. DOI: 10.3390/sym16081036.

[14] Gregor Weihs, Thomas Jennewein, Christoph Simon, Harald Weinfurter, and Anton Zeilinger. Violation of Bell's inequality under strict Einstein locality conditions. *Phys. Rev. Lett.*, 81:5039–5043, 1998. DOI: 10.1103/PhysRevLett.81.5039.

[15] B. Hensen et al. Loophole-free Bell inequality violation using electron spins separated by 1.3 kilometres. *Nature*, 526:682–686, 2015. DOI: 10.1038/nature15759.

[16] Marissa Giustina et al. Significant-Loophole-Free Test of Bell's Theorem with Entangled Photons. *Phys. Rev. Lett.*, 115(25):250401, 2015. DOI: 10.1103/PhysRevLett.115.250401.

[17] J. A. Aguilar-Saavedra, A. Bernal, J. A. Casas, and J. M. Moreno. Testing entanglement and Bell inequalities in H→ZZ. *Phys. Rev. D*, 107(1):016012, 2023. DOI: 10.1103/PhysRevD.107.016012.

[18] Rachel Ashby-Pickering, Alan J. Barr, and Agnieszka Wierzchucka. Quantum state tomography, entanglement detection and Bell violation prospects in weak decays of massive particles. *JHEP*, 05:020, 2023. DOI: 10.1007/JHEP05(2023)020.

[19] Albert M Sirunyan et al. Measurements of production cross sections of the Higgs boson in the four-lepton final state in proton–proton collisions at $\sqrt{s} = 13\,\text{TeV}$. *Eur. Phys. J. C*, 81(6):488, 2021. DOI: 10.1140/epjc/s10052-021-09200-x.

[20] Gordon L. Kane, G. A. Ladinsky, and C. P. Yuan. Using the Top Quark for Testing Standard Model Polarization and CP Predictions. *Phys. Rev. D*, 45:124–141, 1992. DOI: 10.1103/PhysRevD.45.124.

[21] W. Bernreuther, A. Brandenburg, Z. G. Si, and P. Uwer. Top quark spin correlations at hadron colliders: Predictions at next-to-leading order QCD. *Phys. Rev. Lett.*, 87: 242002, 2001. DOI: 10.1103/PhysRevLett.87.242002.

[22] Michele Grossi, Giovanni Pelliccioli, and Alessandro Vicini. From angular coefficients to quantum observables: a phenomenological appraisal in di-boson systems. *JHEP*, 12: 120, 2024. DOI: 10.1007/JHEP12(2024)120.

[23] Marco Fabbrichesi, Roberto Floreanini, Emidio Gabrielli, and Luca Marzola. Bell inequalities and quantum entanglement in weak gauge boson production at the LHC and future colliders. *Eur. Phys. J. C*, 83(9):823, 2023. DOI: 10.1140/epjc/s10052-023-11935-8.

[24] Yoav Afik and Juan Ramón Muñoz de Nova. Entanglement and quantum tomography with top quarks at the LHC. *Eur. Phys. J. Plus*, 136(9):907, 2021. DOI: 10.1140/epjp/s13360-021-01902-1.

[25] Yoav Afik and Juan Ramón Muñoz de Nova. Quantum information with top quarks in QCD. *Quantum*, 6:820, 2022. DOI: 10.22331/q-2022-09-29-820.

[26] Yoav Afik and Juan Ramón Muñoz de Nova. Quantum Discord and Steering in Top Quarks at the LHC. *Phys. Rev. Lett.*, 130(22):221801, 2023. DOI: 10.1103/PhysRevLett.130.221801.

[27] J. A. Aguilar-Saavedra. Tripartite entanglement in H→ZZ,WW decays. *Phys. Rev. D*, 109(11):113004, 2024. DOI: 10.1103/PhysRevD.109.113004.

[28] Rafael Aoude, Eric Madge, Fabio Maltoni, and Luca Mantani. Probing new physics through entanglement in diboson production. *JHEP*, 12:017, 2023. DOI: 10.1007/JHEP12(2023)017.

[29] Alan J. Barr, Pawel Caban, and Jakub Rembieliński. Bell-type inequalities for systems of relativistic vector bosons. *Quantum*, 7:1070, 2023. DOI: 10.22331/q-2023-07-27-1070.

[30] Qi Bi, Qing-Hong Cao, Kun Cheng, and Hao Zhang. New observables for testing Bell inequalities in W boson pair production. *Phys. Rev. D*, 109(3):036022, 2024. DOI: 10.1103/PhysRevD.109.036022.

[31] Daniel Collins, Nicolas Gisin, Noah Linden, Serge Massar, and Sandu Popescu. Bell Inequalities for Arbitrarily High-Dimensional Systems. *Phys. Rev. Lett.*, 88(4):040404, 2002. DOI: 10.1103/PhysRevLett.88.040404.

[32] Dagomir Kaszlikowski, L. C. Kwek, Jing-Ling Chen, Marek Żukowski, and C. H. Oh. Clauser-horne inequality for three-state systems. *Phys. Rev. A*, 65:032118, Feb 2002. DOI: 10.1103/PhysRevA.65.032118. URL https://link.aps.org/doi/10.1103/PhysRevA.65.032118.

[33] Paul Langacker. *The Standard Model and Beyond*. Series in High Energy Physics, Cosmology, and Gravitation. CRC Press, Taylor & Francis Group, Boca Raton, FL, 2nd edition, 2021. ISBN 978-1-4987-6321-9. DOI: 10.1201/822175. URL https://library.oapen.org/handle/20.500.12657/50890.

[34] Stefan Wunsch. SMHiggsToZZTo4L dataset in reduced NanoAOD format for education and outreach. CERN Open Data Portal, 2021. URL https://opendata.cern.ch/record/12361. Accessed: November 21, 2024.

[35] Stefan Wunsch. ZZTo2e2mu dataset in reduced NanoAOD format for education and outreach. CERN Open Data Portal, 2021. URL https://opendata.cern.ch/record/12364. Accessed: November 21, 2024.

[36] Philip M. Pearle. Hidden-variable example based upon data rejection. *Phys. Rev. D*, 2:1418–1425, 1970. DOI: 10.1103/PhysRevD.2.1418.

[37] Jan-Åke Larsson and Richard Gill. Bell's inequality and the coincidence-time loophole. *EPL*, 67:707–713, 2004. DOI: 10.1209/epl/i2004-10124-7.

[38] D. Bohm and Y. Aharonov. Discussion of Experimental Proof for the Paradox of Einstein, Rosen, and Podolsky. *Phys. Rev.*, 108:1070–1076, 1957. DOI: 10.1103/PhysRev.108.1070.